Longitudinal phase space tomography and its implementation in energy recovery linacs

H. Loos

SLAC, 2575 Sand Hill Road, Menlo Park, CA 94025, USA

Abstract

Applying tomographic techniques to study the longitudinal phase space of the electron beam in future energy recovery linacs presents a challenge as it requires nondestructive diagnostics and the manipulations of the phase space are restricted by the energy recovery. The different methods of tomographic reconstruction and previous experiments at the BNL DUV-FEL facility are presented. Different schemes to utilize tomography for an ERL are proposed, including nondestructive transverse and longitudinal beam profile measurements and the necessary phase space transformations to generate the tomographic projections.

Key words: energy recovery linac, beam diagnostics, longitudinal phase space, tomographic reconstruction

PACS: 41.75.Ht, 29.27.Bd, 42.30.Wb

Email address: loos@slac.stanford.edu (H. Loos).

Work supported by Department of Energy contract DE–AC02–76SF00515

1 Introduction

The concept of energy recovery linacs (ERL) makes much higher average beam currents possible than what can be achieved with conventional linear accelerators because the energy stored in the accelerated beam is almost entirely recovered as rf power by recirculating the beam back into the accelerating structure at the opposite phase. This scheme has been demonstrated as a driver for a high power infrared FEL with several mA of average beam current [1] and is proposed for 4th generation light sources [2] and electron-cooling of ion beams [3].

The operation and optimization of an ERL machine requires detailed measurements of the electron beam properties. These measurements are challenging because the necessary energy recovery of the beam permits only the use of non-interceptive diagnostics. Measuring the longitudinal beam phase space properties enables a better understanding of the energy recovery process and the bunch compression and decompression within the recirculating loop. Longitudinal phase space tomography [4–7] has been demonstrated as a tool to characterize this distribution in detail for linear accelerators where interceptive methods are applicable.

This paper is organized into an overview on tomographic methods, recent applications at the BNL DUV-FEL, various possible implementations of tomography at ERLs, and a summary.

2 Longitudinal phase space tomography

The basic idea behind tomographic reconstruction methods is to measure one-dimensional projections of a two-dimensional distribution under different angles of observation or after applying different transformations to the distribution. In the case of the longitudinal time-energy distribution of an electron beam, the procedure is to apply a time-energy chirp with an accelerating structure set to different phases or gradients and then to measure the resulting energy spectrum in a dispersive section of the accelerator. From the reconstructed phase space the slice energy spread, the time-energy correlation, and the beam current distribution can be extracted. The method is inherently a multi-shot technique because the set of projections cannot be measured at once and therefore requires a stable and reproducible beam. No additional instrumentation besides a spectrometer is needed. However, this limits the locations where the phase space distribution can be reconstructed to the entrance of the accelerating structure used to apply the chirp.

The main three reconstruction techniques, filtered back-projection (Radon transform), algebraic reconstruction technique (ART) [8], and maximum entropy method (MENT) [9,10] are based on the beam transport map between the location where the phase space is reconstructed and where the projections are measured. The filtered back-projection is defined for a full set of rotations of a geometric object. The beam transformations therefore have to be described as rotations. If the transformations are created by a varying chirp only, the limited angle of rotations makes extrapolations necessary. The two other methods can be formulated for arbitrary linear and nonlinear transformations and they work with incomplete sets of projections. Due to their

iterative algorithms, prior knowledge of the distribution and constraints on the solution can be implemented.

2.1 Algebraic reconstruction method

The two-dimensional distribution is defined as an image with density values g_l for each pixel l. For each projection p_i, a matrix a_i connects the pixels with the bins j in the respective projection i by

$$p_{i,j} = \sum_l a_{i,jl} g_l \ . \tag{1}$$

The matrix a_i itself is calculated from the linear or nonlinear beam transport function. The reconstructed image g is obtained by iterating an initial guess $g^{(0)}$ with

$$g_q^{(k+1)} = g_q^{(k)} + \sum_j \left[a_{i,jq} \left(p_{i,j} - \sum_l a_{i,jl} g_l^{(k)} \right) / \sum_l a_{i,jl} \right] / \sum_j a_{i,jq} \tag{2}$$

for all projections i until convergence is achieved. During the iterations the non-negativeness of the solution g can be forced by setting negative values to zero. However, noise and inconsistencies in the measured projections can lead to streak artifacts in the solution due to the additive nature of the algorithm.

2.2 Maximum entropy method

The maximum entropy method described here is based on the extended MENT algorithm in [10], but generalized from rotations to arbitrary nonlinear transformations. The idea is to find a distribution for the phase space $f(x, y)$ that

generates the measured projections, but minimizes the amount of information in the solution. This is achieved by minimizing the discriminatory function

$$K(f, f^*) = \int f(x,y) \log \frac{f(x,y)}{e f^*(x,y)} \, dx \, dy \tag{3}$$

with $f^*(x,y)$ containing prior knowledge of the solution. The bins j in projection i are modelled from the phase space with

$$m_{ij} = \int \chi_{ij} \left(M_i(x,y) \right) f(x,y) \, dx \, dy \; . \tag{4}$$

The nonlinear map $M_i(x,y)$ transforms the original phase space point (x,y) into the phase space point where the projection is measured. The function $\chi_{ij}(x,y)$ describes a stripe area along the x-direction in the phase space and has a value of one where it contributes to bin j in projection i and of zero otherwise. The solution is expressed as

$$f(x,y) = f^*(x,y) \prod_{i=1}^{N_p} \sum_{j=1}^{N_s} \Lambda_{ij} \chi_{ij}(M_i(x,y)) \; . \tag{5}$$

The parameters Λ_{ij} which maximize the entropy are found by an iterative Gauss-Seidel procedure with $\Lambda_{ij}^{(n+1)} = \Lambda_{ij}^{(n)} m_{ij} / m_{ij}^{(n)}$ for $m_{ij} \neq 0$ and unchanged otherwise. The coefficients $\Lambda_{ij}^{(0)}$ are initialized to zero for $m_{ij} = 0$ and to one otherwise. One cycle of the iteration uses all projections one after the other. The iteration converges after a few cycles. The multiplicative structure of the solution guarantees it to be nonnegative and stripe artifacts like in ART cannot occur.

3 DUV-FEL results

This section gives examples of applying the different measurement and reconstruction methods at the BNL DUV-FEL facility. This accelerator [11] provides a high brightness electron beam generated by a Ti:Sapphire driven photoinjector for a high gain harmonic generation FEL [12]. Two SLAC-type linac sections accelerate the beam to 70 MeV, followed by a chicane bunch compressor and three more sections that provide a maximum beam energy of 250 MeV. A YAG screen after a spectrometer dipole enables high resolution energy measurements. Longitudinal phase space measurements of the uncompressed beam can either be done by varying the phase of the second linac structure about the crest phase and recording the energy, or by zero-phasing the last structure and varying the accelerating gradient. For the compressed bunch only the last method is applicable. In that case, any remaining chirp from the compression has to be removed with the third structure.

The longitudinal beam transport is calculated from the energy gain of $\Delta E = V\cos(\phi_0+\omega t)$ for the reference particle at phase ϕ_0 and rf frequency ω. An expansion up to second order gives for the particle energy $E' = E+k\,t+k_2\,t^2$ with linear chirp $k = -V\omega\sin(\phi_0)$ and second order chirp $k_2 = -\frac{1}{2}V\omega^2\cos(\phi_0)$.

The resolution of the reconstructed phase space depends on the energy resolution of the profiles for the energy distribution, and on the maximum chirp $k_{\max}$ applied for the temporal resolution. For high brightness electron beams, the longitudinal phase space can be considered as a line distribution characterized by slice energy spread, energy-time correlation, and temporal distribution. The slice energy spread $\sigma_{\delta,0}$ then also limits the temporal resolution. It can be

estimated for this case as $\tau = 2\pi\sigma_{\delta,0}/k_{\max}$ [7].

The results for measurements of the longitudinal phase space with the accelerator set up for FEL operation are shown in Figs. 1 and 2. The left and center of Fig. 1 are the phase space of the uncompressed and compressed beam reconstructed with ART. To remove reconstruction artifacts, a 5% level cut on the distribution was applied. The right part shows the reconstruction of the compressed bunch with MENT showing less artifacts without a level cut. Since the uncompressed slice energy spread is about 5 keV, the time resolution can be estimated to 300 fs which is sufficiently small for the uncompressed and compressed rms bunch length of 2.3 ps and 900 fs, respectively. Figure 2 shows the energy-time correlation and beam current calculated from the phase space for the three reconstructions, as well as the cathode drive laser pulse distribution.

In a different experiment, the drive laser was deliberately modulated to study the effect on the electron beam [13]. Figure 3 shows the phase space reconstructed with ART for three different charges of 20, 65, and 180 pC of the uncompressed electron beam at 73 MeV and a laser modulation period of 2 ps. The corresponding temporal distributions can be found in Fig. 4, showing the charge dependent effect of longitudinal space charge forces on the phase space. The time resolution from the maximum applied chirp was 170 fs, which is sufficient to resolve the details of the phase space structure. The main limitation for the maximum chirp, and hence the resolution, was the energy acceptance of the spectrometer screen and the bunch length, i.e., for shorter bunches an equally better time resolution is possible.

4 Implementation in energy recovery linacs

The two main issues to be considered in using longitudinal phase space tomography in an energy recovery linac are the measurement of the longitudinal projections and the necessary phase space manipulations. The longitudinal projection can either be the energy spectrum or the temporal distribution of the beam. To be able to diagnose the beam even at the full beam current, these measurements have to be (almost) nondestructive to maintain the condition for energy recovery of the beam. The same requirement applies to the phase space manipulations. They either have to be within the acceptance of the energy recovery, or they have to be reversed downstream of the measurement. Alternatively, they could only affect a very small fraction of bunches that could be lost. The feasible profile resolution and range of phase space change will ultimately limit the achievable resolution in the phase space reconstruction.

The measurement of the energy distribution is closely related to the development of nondestructive transverse beam profile monitors which will be deployed in dispersive regions in the lattice. They could be synchrotron radiation based, or flying or laser wire profile monitors. Time profiles can be measured likewise by the spectrum of coherent diffraction radiation, electro-optic methods, or with synchrotron radiation detected with a streak camera.

Several options exist for the phase space manipulations. The entire main linac in the ERL or the last structures can be set to various off-crest phases to obtain the phase space distribution at the entrance or inside the linac. The spectrum should be measured in the first dipole downstream. For measurements at other locations, especially of a compressed beam after the first arc, an additional

accelerating structure operated at zero-phase is necessary. For a time domain measurement, the beam has to be variably compressed and uncompressed in both arcs, respectively. However, to resolve energy time correlations in the phase space, the beam has to be over-compressed, which limits this method to very low charge beams because of collective effects like CSR or LSC.

To study the applicability and limits of these methods, the parameters of the Cornell Phase I and II ERL proposals [14] were chosen as examples of a low energy (100 MeV) and a high energy (5 GeV) case. The phase space parameters for the 100 MeV case are an energy spread of $\sigma_{\Delta E/E} = 2 \cdot 10^{-4}$ and a bunch length of $\sigma_z = 2\,\mathrm{ps}$. Using synchrotron radiation as transverse profile diagnostics [15] and a dipole bend radius of 1 m, a resolution of 10 μm is possible. Assuming a dispersion of $\eta = 0.5\,\mathrm{m}$, the energy resolution of 2 keV or $2 \cdot 10^{-5}$ is sufficient to resolve the energy structure in the phase space. A maximum chirp of $k_{\max} = 400\,\mathrm{keV/ps}$ can be done with all sections set to 30 degrees off-crest. The resulting beam is still within 2% energy acceptance of the machine. This results in a temporal resolution of 30 fs, which will be larger if the actual slice energy spread is larger than the energy resolution. In the 5 GeV case, the larger bend radii in the order of 10's of meters in a TBA cell limit the resolution from a synchrotron profile monitor to 30 μm. The small dispersion of $\eta = 0.04\,\mathrm{m}$ gives an energy resolution of $7 \cdot 10^{-4}$ which is larger than the energy spread. An energy measurement with sufficiently high resolution would therefore require a specifically designed lattice with a much larger dispersion in the respective dipole. Assuming the energy resolution of the low energy case, the same temporal resolution can be achieved with the main linac set moderately off-crest.

5 Summary

Using only standard instrumentation in high brightness linear accelerators, tomographic reconstruction has been shown to be a useful tool to study the beam dynamics in the longitudinal phase space. However, it can only be applied at specific locations in an accelerator, and one has to be careful about possible collective effects that might alter the results. Higher order beam transport maps can be implemented in a consistent way without the need to invert these maps in the reconstruction algorithm for both ART and MENT. This is an important feature for ERLs where these higher order terms become relevant.

The implementation in an energy recovery linac requires the energy spectrum of the recirculating beam to be measurable with proper resolution and that the machine has a sufficient phase tuning range and energy acceptance. For GeV ERLs these issues should already be considered in the design of the machine.

6 Acknowledgements

The author wishes to thank his colleagues B. Sheehy, T. Shaftan, Y. Shen, L.H. Yu, X.J. Wang, Z. Wu from BNL and R. Fiorito and J. Neumann from UMD for their help and contribution to the experiments at the BNL DUV-FEL discussed in this paper.

This work was supported by DOE Contracts DEAC No. DE-AC02-98CH10886 and DE-AC03-76SF00515.

References

[1] G.R. Neil et al., Phys. Rev. Lett. 84 (2000) 662

[2] I. Bazarov et al., CHESS Technical Memo 01-003 and JLAB-ACT-01-04 (2001)

[3] I. Ben-Zvi et al., Proceedings of the 20th Particle Accelerator Conference, Portland, OR, May 2003, p. 39

[4] E.R. Crosson et al., Nucl. Instrum. Meth. A 375 (1996) 87

[5] S. Kashiwagi et al., Proceedings of the XX International Linac Conference, Monterey, CA, 2000, p. 149

[6] M. Hüning, Proceedings of DIPAC 2001, ESRF, Grenoble

[7] H. Loos et al., Nucl. Instrum. Meth. A 528 (2004) 189

[8] A.C. Kak, M. Slaney, Principles of Computerized Tomographic Imaging, IEEE Press, 1979

[9] G. Minerbo, Comput. Graph. Image Processing, 10 (1979) 48

[10] N.J. Dusaussoy, I.E. Abdou, IEEE Trans. Sign. Proc. 39 (1991) 1164

[11] W.S. Graves et al., Proceedings of the 19th Particle Accelerator Conference, Chicago, IL, June 2001, p. 2860

[12] L.H. Yu et al., Phys. Rev. Lett. 91 (2003) 074801

[13] J. Neumann et al., Proceedings of the 2004 Free Electron Laser Conference, Trieste, Italy, September 2004, p. 586

[14] G.H. Hoffstaetter et al., Proceedings of the 20th Particle Accelerator Conference, Portland, OR, May 2003, p. 192

[15] A. Hofmann, Diagnostics with synchrotron radiation, in CERN Accelerator School on Synchrotron Radiation and Free Electron Lasers, CERN 98-04, p. 303

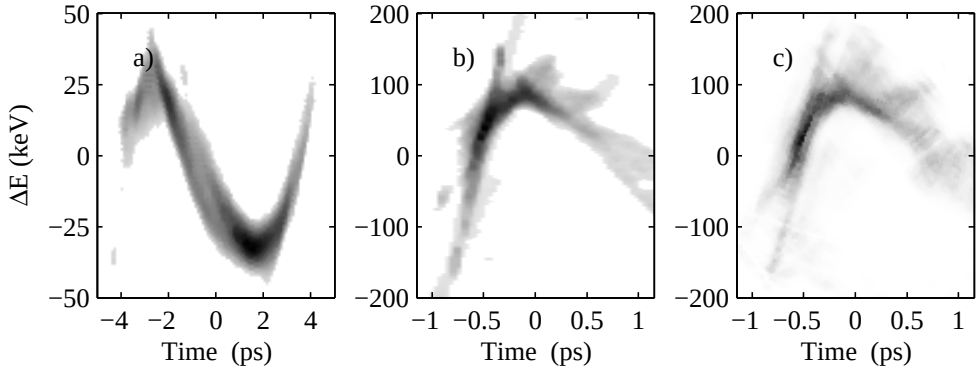

Fig. 1. Reconstructed longitudinal phase space distributions of the DUV-FEL accelerator. Panel a) shows the uncompressed, panels b) and c) the compressed beam. The reconstruction method is ART for a) and b) and MENT for c).

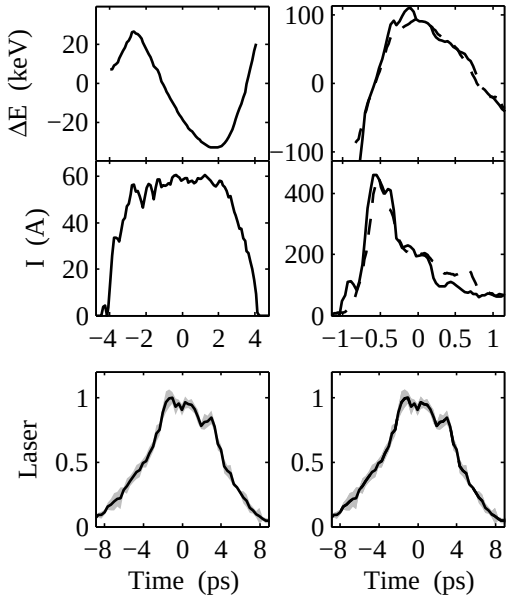

Fig. 2. Temporal distributions corresponding to the reconstruction in Fig. 1. From bottom to top is shown the measured cathode drive laser distribution, the reconstructed electron beam current, and the energy – time correlation. The left part corresponds to the uncompressed, the right part to the compressed beam. The solid curves are based on ART and the dashed on MENT.

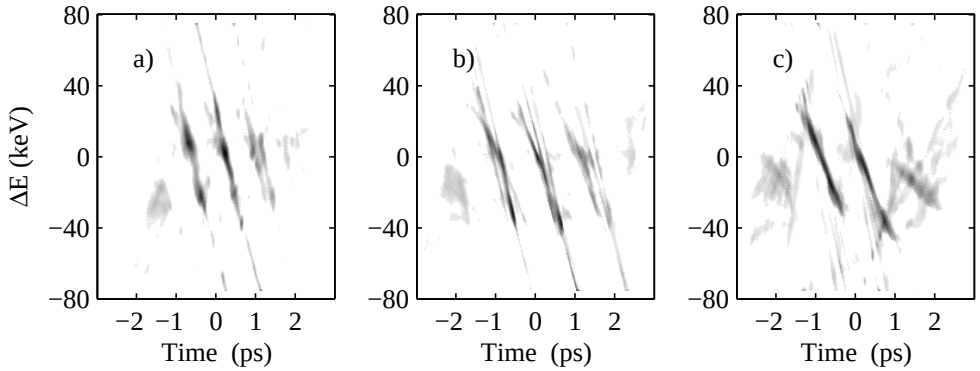

Fig. 3. Longitudinal phase space distributions of the modulated electron beam. From left to right the charge was 20, 65, and 180 pC.

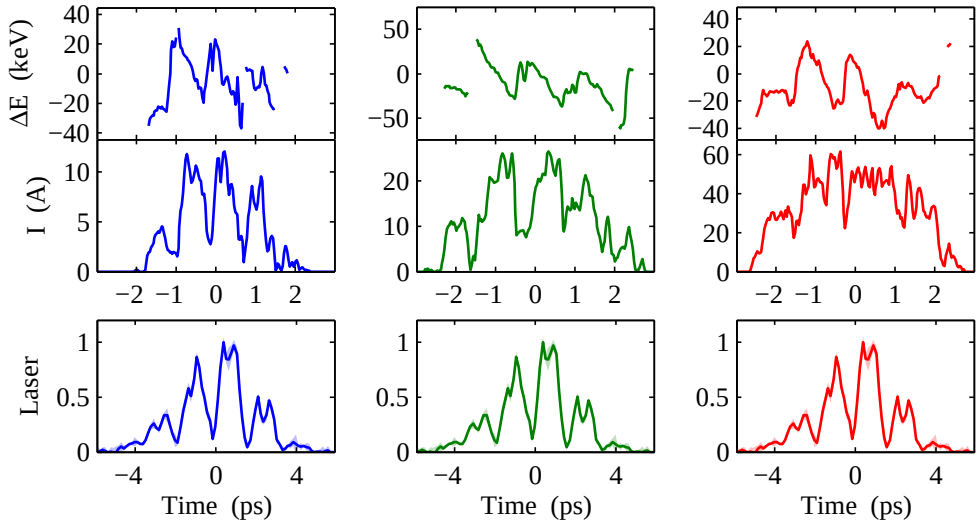

Fig. 4. Temporal distributions corresponding to the reconstruction in Fig. 3 with bunch charges of 20, 65, and 180 pC from left to right.